J Comput Aided Mol Des (2012) 26:1277–1292
DOI 10.1007/s10822-012-9615-5

Virtual and experimental high-throughput screening (HTS) in search of novel inosine 5′-monophosphate dehydrogenase II (IMPDH II) inhibitors

Torsten Dunkern · Arati Prabhu · Prashant S. Kharkar · Heike Goebel · Edith Rolser · Waltraud Burckhard-Boer · Premkumar Arumugam · Mahindra T. Makhija

Received: 10 August 2012 / Accepted: 24 October 2012 / Published online: 2 November 2012

Abstract IMPDH (Inosine 5′-monophosphate dehydrogenase) catalyzes a rate-limiting step in the de novo biosynthesis of guanine nucleotides. IMPDH inhibition in sensitive cell types (e.g., lymphocytes) blocks proliferation (by blocking RNA and DNA synthesis as a result of decreased cellular levels of guanine nucleotides). This makes it an interesting target for cancer and autoimmune disorders. Currently available IMPDH inhibitors such as mycophenolic acid (MPA, uncompetitive inhibitor) and nucleoside analogs (e.g., ribavirin, competitive inhibitor after intracellular activation by phosphorylation) have unfavorable tolerability profiles which limit their use. Hence, the quest for novel IMPDH inhibitors continues. In the present study, a ligand-based virtual screening using IMPDH inhibitor pharmacophore models was performed on in-house compound collection. A total of 50,000 virtual hits were selected for primary screen using in vitro IMPDH II inhibition up to 10 μM. The list of 2,500 hits (with >70 % inhibition) was further subjected to hit confirmation for the determination of IC_{50} values. The hits obtained were further clustered using maximum common substructure based formalism resulting in 90 classes and 7 singletons. A thorough inspection of these yielded 7 interesting classes in terms of mini-SAR with IC_{50} values ranging from 0.163 μM to little over 25 μM. The average ligand efficiency was found to be 0.3 for the best class. The classes thus discovered represent structurally novel chemotypes which can be taken up for further development.

Keywords Inosine 5′-monophosphate dehydrogenase · IMPDH · Pharmacophore screening · Virtual screening · HTS

Electronic supplementary material The online version of this article (doi:10.1007/s10822-012-9615-5) contains supplementary material, which is available to authorized users.

T. Dunkern · H. Goebel · E. Rolser · W. Burckhard-Boer
Global Discovery, Nycomed: A Takeda Company, Nycomed GmbH, Byk-Gulden-Str. 2, 78467 Constance, Germany

Present Address:
T. Dunkern
Global Drug Discovery, Grünenthal GmbH, 52099 Aachen, Germany

A. Prabhu · P. S. Kharkar · M. T. Makhija (✉)
Global Discovery, Nycomed: A Takeda Company, Plot 29-31, Suren Road, Andheri (E), Mumbai 400093, India
e-mail: makhijatm@yahoo.co.in;
Mahindra.Makhija@takeda.com

Present Address:
A. Prabhu
Piramal Life Sciences, 1 Nirlon Complex, Goregaon (E), Mumbai 400063, India

Present Address:
P. S. Kharkar
SPP School of Pharmacy and Technology Management, SVKM's NMIMS University, V. L. Mehta Road, Vile Parle (W), Mumbai 400056, India

P. Arumugam
GVK Biosciences Private Limited, Plot No. 28A, IDA Nacharam, Hyderabad 500076, India

Introduction

High-throughput screening (HTS) is a method of choice in the initial stages of lead discovery in the pharmaceutical industry [1, 2]. In a typical HTS campaign, in-house compound collections are evaluated in a primary assay at a single concentration. The so-called hits (meeting a predefined criterion such as % inhibition) are screened further in a process known as 'hit confirmation'. 'Frequent hitters' or

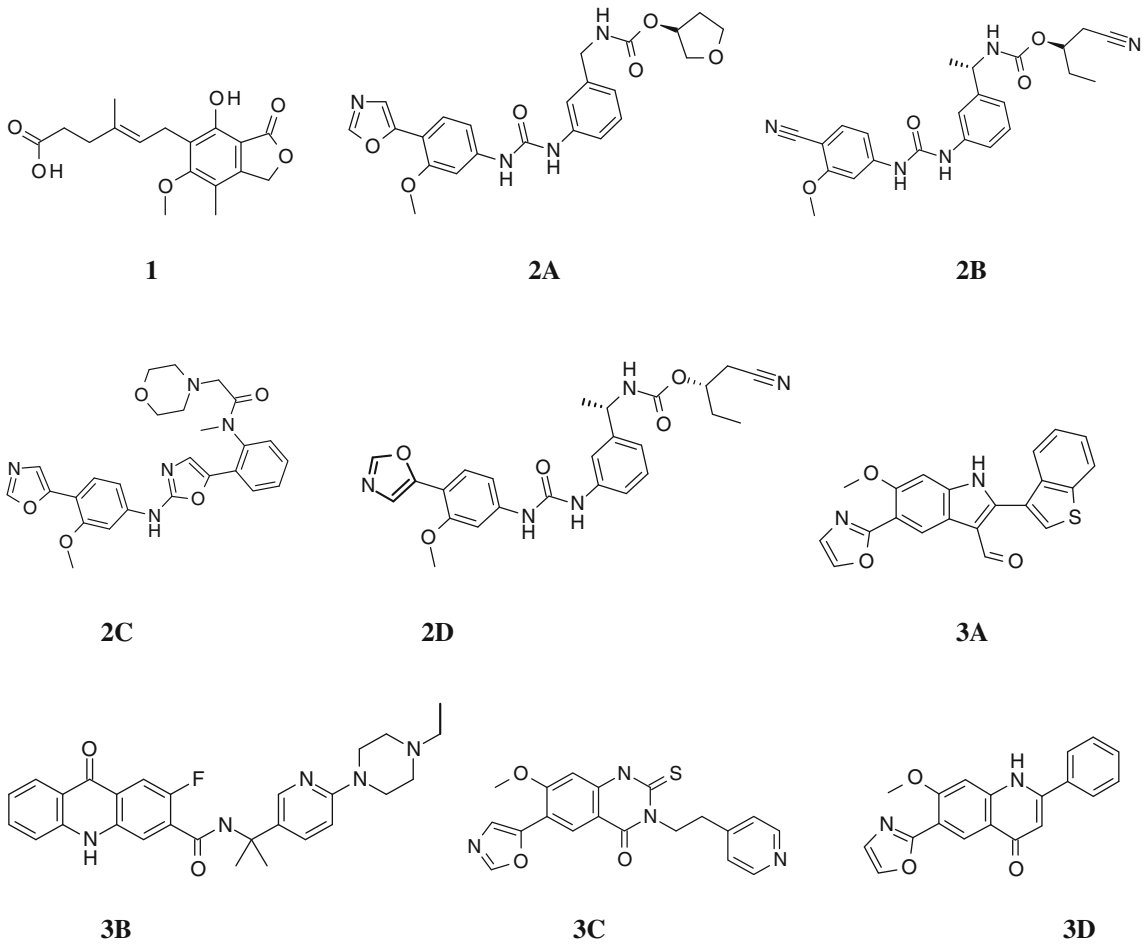

Fig. 1 Structures of some IMPDH Inhibitors used for the development of 5-point pharmacophore model

false positives are weeded out in this and subsequent HTS work-up. Careful inspection of the hits with the aim of finding or observing mini-structure–activity relationships (mini-SAR) usually leads to a suitable starting point for a conventional medicinal chemistry program. Virtual (structure-based or ligand-based) HTS (vHTS) prior to its experimental counterpart is one of the most sought-after strategies to optimize resource utilization during the actual HTS. Many researchers tend to use either or both the structure- and ligand-based approaches for vHTS in order to compliment the capabilities of molecular modeling and cheminformatics softwares, which are used for such applications [3, 4]. In brief, HTS (virtual and experimental), despite several shortcomings or limitations, continues to enjoy the status of preferred method of lead discovery in the pharmaceutical industry.

In a similar attempt, we have utilized the virtual and experimental HTS methods for finding novel non-nucleoside lead structures as inhibitors of inosine monophosphate dehydrogenase (IMPDH, EC 1.1.1.205). This enzyme exists in two isoforms—I and II, and plays a pivotal role in de novo biosynthesis of guanine nucleotides. It converts inosine-5′-monophosphate (IMP) to xanthosine-5′-monophosphate (XMP) which depends on nicotinamide adenine dinucleotide (NAD) cofactor [5, 6]. Inhibition of IMPDH is an important strategy leading to reduced cellular levels of guanine nucleotides, thereby producing antiproliferative effect [7]. Several autoimmune diseases are characterized by proliferating B and T lymphocytes, which in turn, rely on constant supply of guanine nucleotides via IMPDH-catalyzed reaction. Hence, the inhibition of IMPDH sequesters this proliferation of lymphocytes, thereby producing immunosuppression [8]. Other effects and consequences therein of IMPDH inhibition are covered elsewhere [9].

Mycophenolic acid (MPA) (**1**, Fig. 1) is a long-known potent, reversible and uncompetitive IMPDH inhibitor. Mycophenolate mofetil (MMF, CellCept®), a N-morpholinoethyl ester prodrug of MPA, has been approved for the treatment of acute allograft rejection following kidney transplant [10]. MPA and its derivatives [MMF or MPA sodium (Myfortic®)] cause dose-limiting gastrointestinal (GI) toxicity in addition to their metabolic liability. Thus, high doses (CellCept®, 1 g b.i.d. and Myfortic®, 720 mg

b.i.d.) are required to maintain the therapeutic plasma levels. Other IMPDH inhibitors which are nucleoside analogs e.g., Mizoribine (Bredinin®) and Ribavirin (Virazole®), etc., compete with IMP (substrate) after intracellular phosphorylation, and thus act as competitive IMPDH inhibitors. These too have unfavorable tolerability profiles [7]. A significant number of non-nucleoside inhibitors of IMPDH are reported in the literature (crossref 10-37 in Ref. [13, 26]). Despite the availability of several potent IMPDH inhibitors (Fig. 1), the quest for newer, safer, potent and orally bioavailable inhibitors continues owing to the involvement of the target in several disease states.

The present study highlights our efforts to develop novel non-nucleoside IMPDH inhibitors devoid of the side effect profiles of MPA or related drugs. In this study we describe—(a) the pharmacophore model development using structurally diverse and potent non-nucleoside IMPDH inhibitors reported in the literature, (b) the use of the pharmacophore model along with other approaches such as fingerprint (FP) screening, for the virtual screening of in-house compound collection to prioritize compounds for HTS, (c) the HTS and its work-up, (d) the confirmation of hits followed by (e) thorough analyses of the HTS results (clustering, visual inspection, etc.). These novel inhibitors can be potentially useful in several diseases/disorders with deregulated immune component at the core, including arthritis, inflammatory bowel disease, psoriasis, dermatitis, prevention of transplant rejection and many others.

Experimental section

Hardware and software

All the molecular modeling studies described herein were performed on a Hewlett-Packard xw4600 computer workstation with 2 GB memory and Intel Core® 2 Duo processors of 2.66 GHz each running under Red Hat Enterprise Linux Version 5. The molecular modeling operations were performed using Schrödinger suite 2011 [11].

Pharmacophore development

The structures of IMPDH inhibitors used for the development of pharmacophore hypotheses with IC_{50} values ranging from 6 to 30 nM are shown in Fig. 1. A docking protocol using Chinese hamster (*Cricetulus griseus*) IMPDH II crystal structure (PDB ID 1JR1) [12] and Glide, version 5.7 was developed. Monomer of IMPDH II with covalently bound XMP (E-XMP*) was used as the starting structure. Initial runs were performed using the crystal structure ligand **1** (Fig. 1). The docking protocol using Glide XP (Extra Precision) mode outperformed Glide SP (Standard Precision) in terms of docking scores and reproducing the binding mode observed in the crystal structure (Table 1). Hence, Glide XP was used for docking the reference compounds to generate the starting conformations to be used for the pharmacophore development. The binding modes of four reference compounds (**1**, **2A**, **2B** and **2D**, Fig. 1) are shown in Fig. 2a–d. Most of the top-ranked conformations of the reference compounds conserved key binding interactions with the IMPDH II enzyme [13]. These are discussed in detail in the Results and Discussion section. The docked conformations of the inhibitors (Fig. 1) were used as such for the pharmacophore development using Phase, version 3.3 [14, 15]. The ligand poses from the docking runs were imported and subjected to the pharmacophore model development process without enumerating additional conformations. The common features were searched followed by scoring the hypotheses. The scoring process identifies the best candidate hypothesis and provides an overall ranking of all hypotheses. The scoring algorithm employed in Phase takes into consideration the alignment of site points and vectors, selectivity, volume overlap, number of ligands matched, relative conformational energy and activity [14, 15]. The top-scoring hypothesis consisting of 5 features (AAADR) was selected

Table 1 In vitro inhibition data (literature and in-house) and the docking scores of the reference compounds [standard precision (SP) and extra precision (XP)] in IMPDH II (PDB ID 1JR1)

Reference compound	Literature K_i [5–8]	Literature IC_{50} [5–8]	In-house IC_{50}	SP score	XP score
1 (MPA)	6–10 nM	11–1,500 nM	100 nM	−10.524	−11.722
2A (VX-497)	10 nM	7–10 nM	22 nM	−7.277	−8.976
2D (VX-944)	6 nM	–	7.9 nM	−7.828	−10.153
2B (VX-148)	6 nM	–	380 nM	−7.249	−10.108
2C (BMS-337197)	3.2 nM	–	ND[a]	−7.884	−9.971
3A (BMS-338259)	–	30 nM	ND[a]	−8.076	−8.930
3B (BMS566419)	–	17 nM	ND[a]	−6.158	−7.922
3C (UCB393197)	–	13 nM	ND[a]	−7.658	−7.424

[a] *ND* not determined

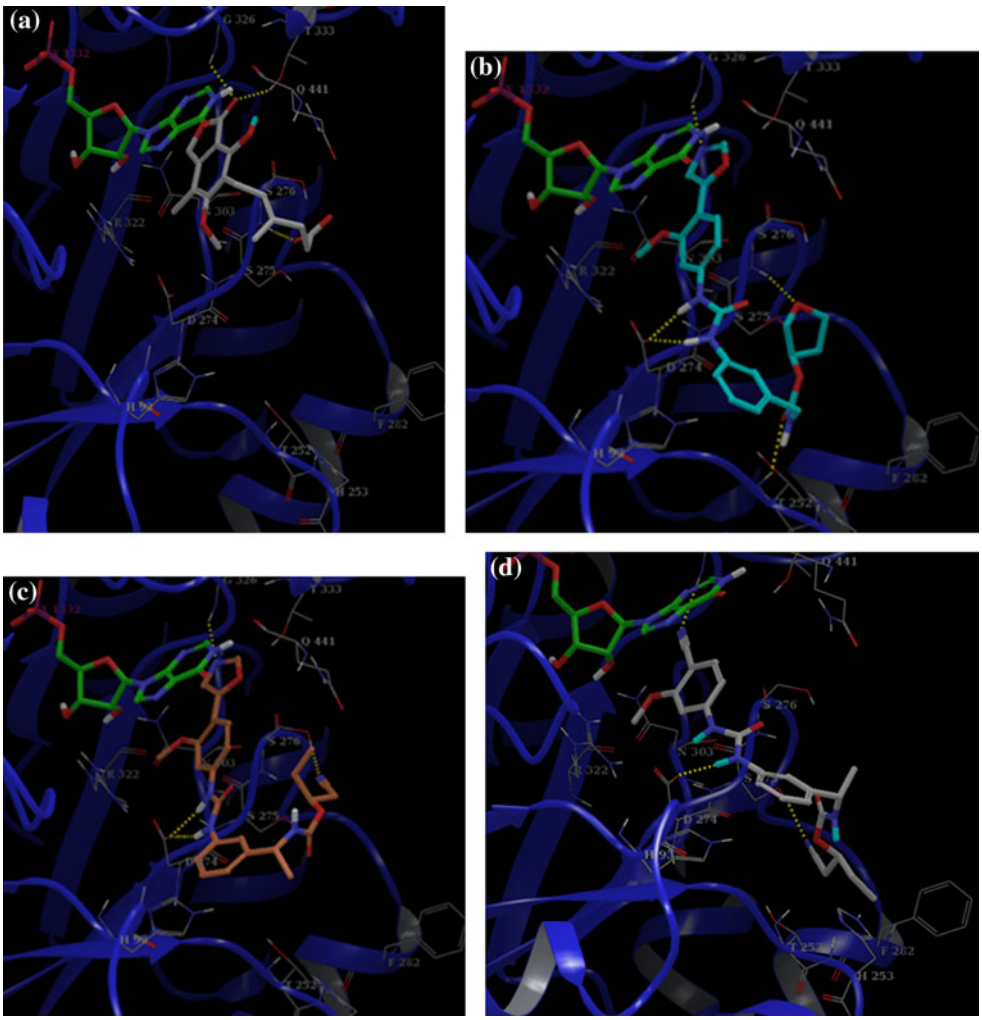

Fig. 2 The docked poses of reference compounds **1** (MPA) (**a**), **2A** (VX-497) (**b**), **2D** (VX-944) (**c**) and **2C** (VX-148) (**d**) bound to IMPDH II (PDB ID 1JR1). Covalently bound IMP thioimidate intermediate XMP (XMP*) is shown as ball-and-stick model with carbon atoms colored *green* and the inhibitors are shown as ball-and-stick models with carbons atoms colored *cyan* (a), light brown (b) and light grey (c)

for the ligand-based virtual screening based on alignment score, volume score and selectivity. The features of this hypothesis represent the key binding interactions observed in the docked conformations of the reference compounds. Other top-scoring hypotheses which lacked such features were not considered (Fig. 2).

Virtual screening using 3D pharmacophore

The in-house collection of ~500,000 compounds was used for virtual screening using the 3D pharmacophore model. A Phase database was generated by ionizing the structures at pH 7.0 ± 2.0 using Epik, removing high energy states, reactive functional groups and duplicate structures. The maximum number of conformations was set to 100 and only up to 10 conformations were allowed per rotatable bond. The generated Phase database was then screened for compounds matching the pharmacophore hypothesis. The hits were subsequently filtered and ranked according to specified criteria such as fitness score [14, 15]. Two types of searches were performed—with stringent constraints and loose constraints. For stringent constraints, the distance matching tolerance was set to 1.0 Å along with a must match at least 4 site points. In the advanced matching options, all the site tolerances were set to 1.0 Å. In case of loose constraints, a distance tolerance of 2.0 Å and a must match at least 3 site points options were used in addition to other default settings.

Virtual screening using 2D fingerprints

In addition to 3D pharmacophore search, few 2D FPs were also used for virtual screening (Fig. 3) such as (a) dendritic FPs (Canvas [16, 17]), (b) MOLPRINT2D (Canvas), (c) topological FPs (FTrees[18, 19]) and (d) similarity FPs (SpotFire [20]). Of the several FPs in Canvas 1.4, only dendritic and MOLPRINT2D were selected since these FPs performed better than others in some large scale screening studies [17, 21]. FTrees is a highly efficient software for fuzzy similarity searching. The topological descriptor (Feature Tree) captures the connectivity and physico-chemical properties of functional groups and imparts

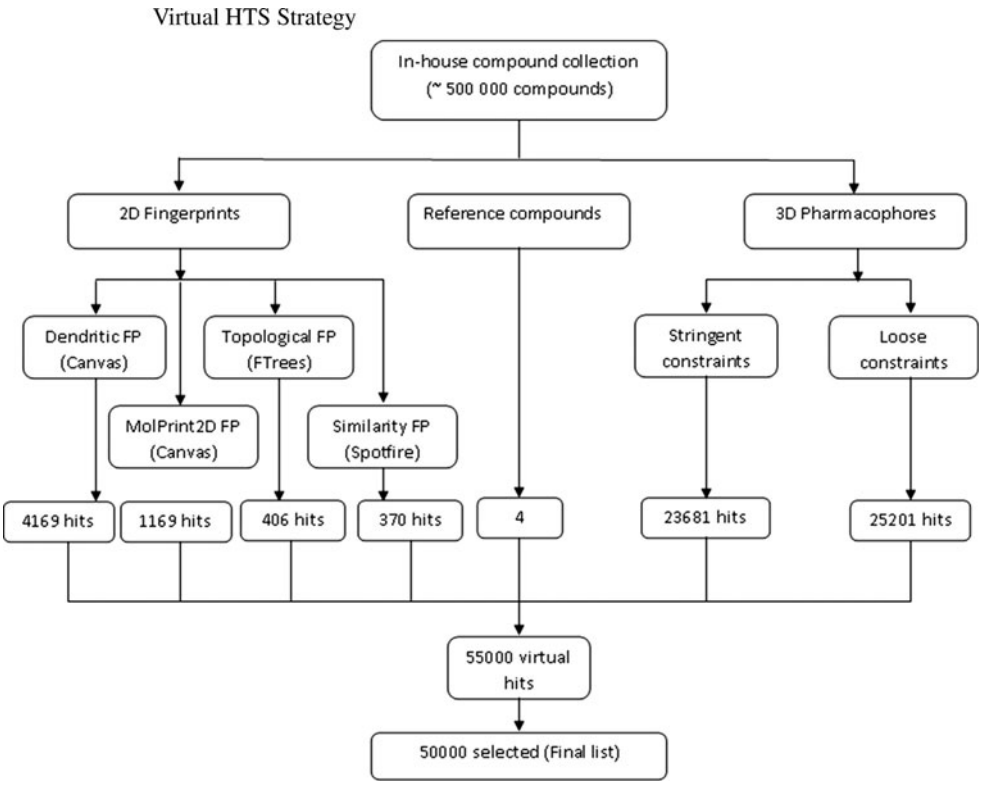

Fig. 3 Virtual HTS strategy

FTrees an unique capability of detecting novel molecular scaffolds [18, 19]. All the compounds used for developing pharmacohore hypothesis were used as reference for similarity searching using 2D fingerprints. The database (in-house compound collection) used for the 2D FP-based virtual screening was filtered to remove compounds which were not drug-like (including compounds with reactive functional groups) using Canvas. The details of virtual screening such as criteria (pharmacophore and 2D FPs) and the corresponding number of virtual hits are shown in Fig. 3. Of the 9 reference compounds (Fig. 1), four (**1**, **2A**, **2B** and **2D**) were included in the final hit list. A total of 55,000 virtual hits were pooled using 3D pharmacophore and 2D FP searches. This was subsequently reduced to 50,000 compounds after checking the redundancy and availability of actual samples in our compound collection. These 50,000 compounds were used for the primary screening against IMPDH II at 10 μM.

High-throughput screening

cDNA coding for IMPDH II (Accession number BC0155) was obtained from Open Biosystems in pOTB7 vector. *Escherichia coli* DH5α, *E. coli* DE3 (BL21) and plasmid pET-21b were purchased from Novagen. Restriction enzymes, Pfu DNA Polymerase, DNA marker were purchased from NEB. Plasmid DNA purification kit was purchased from Qiagen. Oligonucleotides, Sephadex G-25 column procured from GE. Isopropyl β-D-1-thiogalactopyranoside (IPTG), Protease inhibitor cocktail, Inosine monophosphate (IMP), Nicotinamide Adenosine Dinucleotide (NAD), Guanine Mono phosphate (GMP), Mycophenolic acid (MPA) and routine chemicals were obtained from Sigma-Aldrich. The 384-well plate for UV assay was purchased from Corning. SpectraMax plus 384 (Molecular Devices, Sunnyvale, CA, USA).

Cloning

The cDNA was amplified by PCR using forward primer-CGTCAAGCTTATGGCCGACTACCTG and Rev—AGCTGACCTCGAGGAAAAGCCGCTTCTC (SIGMA) designed to incorporate restriction enzyme sites *Hin*dIII and *Xho*I to 5′ and 3′ ends, respectively. PCR amplified full length IMPDH II was ligated with *Hin*dIII/*Xho*I (NEB) digested pET21b expression vector (Novagen). The presence of insert was confirmed by restriction digestion followed by automated DNA sequencing.

Expression and purification

The plasmid containing the desired gene insert, pET21b-IMPDH II, was transformed into BL21 (DE3), E. coli cells, which were then grown in LB broth containing ampicillin. Protein expression was induced by 0.3 mM IPTG (Isopropyl 1-thio-D-galactopyranoside) at 0.3–0.4 OD_{600},

27 °C, for 5 h. Purification was performed by suspending the cell pellets in 50 mM Potassium phosphate buffer pH 7.4, 1 M DTT containing protease inhibitor cocktail and lysing them by sonication. The clarified whole cell lysate was subjected for 25 % ammonium sulphate fractionation (weight/volume). The fractionated IMPDH II in pellet was suspended in 100 mM potassium phosphate buffer pH 7.4, 0.5 mM EDTA and 1 mM DTT, and subjected for desalting using Sephadex G-25 column on AKTA explorer.

Enzyme assay and compound screening

For HTS screen, assays were performed in duplicate in 384-well, UV-transparent, polystyrene, clear flat bottom micro plates (Corning 3675) in a reaction volume of 40 µl. Compounds were incubated with 0.75 µg of enzyme for 15 min at 37 °C in assay buffer (50 mM Tris–HCl (pH 8.0), 100 mM KCl, 3 mM EDTA, and 1 mM dithiothreitol containing 4 % DMSO. For compound auto fluorescence assessment an initial absorbance was measured at 340 nm using Spectromax plus 384 plate reader. Later the reaction was initiated by adding IMP and NAD at a final concentrations of 300 and 500 µM respectively. Plates were incubated for 50 min and reaction was terminated by adding 15 mM GMP and the production of NADH was determined by reading the plates at 340 nM. Changes in absorbance were determined by subtracting the initial absorbance value from the final absorbance. For primary screening 10 µM of test compounds in duplicates were tested in 384-well plate format. Mycophenolic acid (MPA) at 10 µM was used as a positive control and no inhibitor as a vehicle control.

Results and discussion

The present study details the virtual and experimental HTS in an effort to discover novel small molecule non-nucleoside IMPDH inhibitors. For virtual screening, we had two choices—structure-based and ligand-based approaches. There are several IMPDH II crystal structures deposited in the Protein Data Bank. Most of these structures contain substrate (IMP), substrate analogs (e.g., 6-chloro-IMP) or prodrugs (which upon metabolic activation are converted into nucleotides, e.g., ribavirin) as ligands. These structures containing substrate or substrate analogs were not considered for the structure-based vHTS. Of the 26 structures of IMPDH in PDB, 10 (1 from Chinese hamster, 2 from bacteria, 6 from Tritrichomonas suis and 1 human structure which is yet to be published) contain clinically used inhibitor MPA, which inhibits IMPDH by acting as a replacement for the nicotinamide portion of the cofactor NAD and a catalytic water molecule. There are significant structural and kinetic differences between microbial and human enzymes. In terms of sequence similarity, the closest match (>95 % sequence similarity) was the structure from Chinese hamster *C. griseus* (PDB ID 1JR1). Pilot runs of vHTS using docking analyses performed on in-house compound collection did not yield satisfactory results in terms of number of hits (data not shown). Hence, we decided to opt for ligand-based vHTS approach using 3D pharmacophore and 2D fingerprint-based screening. The ligand-based virtual screening protocol started with the selection of reference compounds based on potency and structural diversity. These served as starting points for developing 3D pharmacophore models and similarity searching. The complete list of the reference compounds is given in Fig. 1. The first compound we selected was the prototype IMPDH inhibitor, mycophenolic acid (**1**). The second group comprised of biaryl urea [VX-497 (**2A**), VX-148 (**2B**) and VX-944 (**2D**)] and urea isosteres [BMS-337197 (**2C**)]. The third group consisted of compounds containing bi- or tricyclic cores such as indole (BMS-338259, **3A**), acridone (BMS-566419, **3B**), quinazoline thione (UCB-393197, **3C**) and quinolone (**3D**). The IC_{50} values (literature and in-house) of these reference compounds along with their corresponding docking scores (Standard Precision, SP and Extra Precision, XP) are given in Table 1. The ranges of common molecular properties of these reference compounds were—molecular weight: 319.33–489.52; topological polar surface area (TPSA): 51.22–136.27; H-bond acceptors: 5–10; H-bond donors: 1–3. All the reference compounds were docked in the crystal structure of Chinese hamster IMPDH II (PDB ID 1JR1) enzyme using Glide 5.7 [22–25]. The docking modes of **1**, **2A**, **2B** and **2D** are shown in Fig. 2. The binding modes of all the reference compounds were similar (except 1) with common H-bonding interaction of a central –NH– (part of urea, amide of bicyclic heterocycle) with Asp274. In addition, the phenyl ring bearing $–OCH_3$ substituent formed pi–pi stacking with purine core of covalently bound IMP thioimidate intermediate (XMP^*) and the $–OCH_3$ substituent was found to stabilize in a small pocket lined by Arg322, Asn303 and Asp364. Also, N of oxazole (present in **2A**, **2C**, **2D**, **3A**, **3C**) or CN (**2B**) present on the $–OCH_3$–bearing phenyl ring formed an H-bond with the backbone –NH– of Gly326. These key binding interactions observed in the docked conformations are in line with the experimental binding modes as seen in [13]. This critical information helped us in the selection of appropriate pharmacophore hypothesis.

3D pharmacophore based virtual screening

Figure 4 depicts the top-scoring 5-point pharmacophore hypothesis—AAADR—with interfeature distances and the corresponding feature alignment onto 2 reference compounds

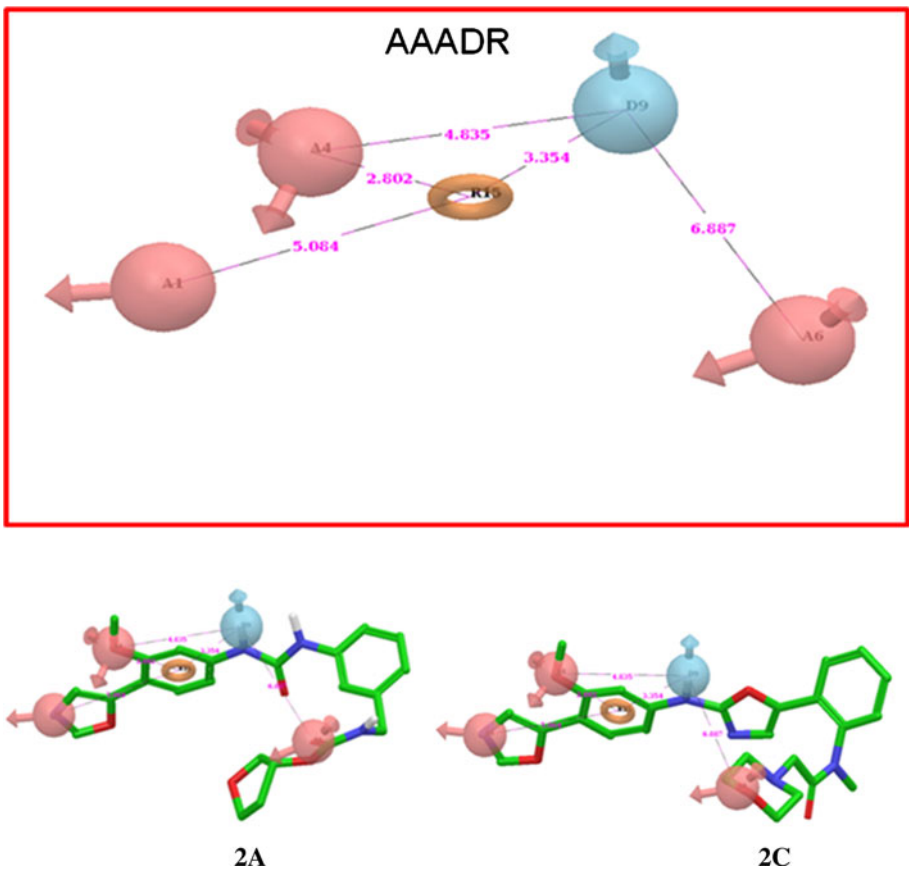

Fig. 4 3D Pharmacophore Model—AAADR—used for ligand-based virtual screening with corresponding feature alignment onto 2 reference compounds

2A and **2C**. The donor feature (D) mimics the key H-bonding interaction exhibited by the central –NH– part. The two proximal AA (acceptor) features represent $–OCH_3–$ and N of oxazole or –CN present on the proximal phenyl ring (feature R). The remaining A feature represents the –CO of carbamate or other related H-bond acceptors (aliphatic –CN, morphine O, tetrahydrofuran O, etc.). This hypothesis was one of the top-rank hypotheses in terms of related scores such as alignment score, volume overlap, number of site points matched, etc. (data not shown). The 3D pharmacophore-based virtual screening was initiated using the selected hypothesis (AAADR).

Initially, a pilot run was tried in order to optimize the virtual screening parameters. The tolerance for intersite distance was tried at 0.5, 1.0 and 2.0 Å along with a must match on at least 4/5 features. The combination of distance tolerance 0.5 Å and 5 feature match yielded very few hits. It was then decided to use two types of constraints—stringent and loose. The combination, distance tolerance of 1 Å and a must match on at least 4 features, formed stringent constraints, and distance tolerance of 2 Å in combination with at least 3 features served as loose constraints. Subsequent searches using these pharmacophoric constraints resulted in 23,681 (stringent constraints) and 25,201 (loose constraints) hits. It was expected that the hit list with loose constraints might have some overlapping hits from the hit list generated using stringent constraints. No attempt was made to remove duplicates, if any, from the combined hit list (48,882) at this stage.

2D fingerprint based virtual screening

In contrast to methods which rely on target structure or 3D shape, such as docking, FP-based methods completely ignore any explicit information about ligand-receptor interactions. A large variety of choices is available in terms of fragmentation schemes, atom/bond typing, similarity indices, etc. Of the 4 FPs we used, dendritic FPs encode both linear and branched features with no special treatment of rings, whereas MOLPRINT2D FPs encode atom environments using lists of atom types located at different topological distances.[12b] In case of both FPs in Canvas 1.4 (dendritic and MOLPRINT2D) our attempts to use a similarity cut-off of 0.5 resulted in quite low number of hits (data not shown). Other values between 0.2 and 0.5 did not lead to any further improvement in the number of hits. Hence, a similarity cut-off of 0.2 was used to include more compounds with great structural diversity. Another reason for using such a low cut-off can be attributed to the nature of in-house compound collection. For topological FPs (FTrees), the

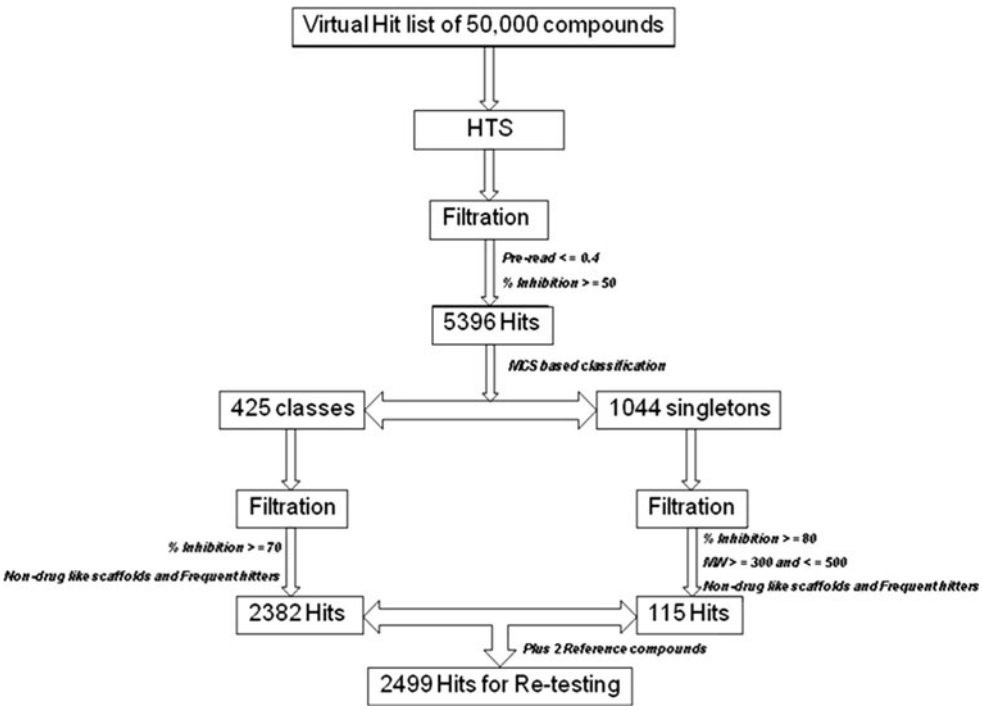

Fig. 5 HTS Work-up

cut-off value of 0.88 was used and for similarity FPs (Spotfire), the cut-off value was set to 0.5. The highest number of hits (4,169) were obtained from screening using dendritic FPs, followed by MOLPRINT2D (1,169), FTrees (406), and Spotfire (370). The virtual hit list pooled from pharmacophore and FP-based searches contained a total of 55,000 compounds which were subjected to duplicate removal and compound availability check. Finally, 50,000 compounds were selected for experimental HTS of IMPDH II inhibition at 10 μM concentration.

HTS work-up

The HTS assay was performed by measuring the conversion of NAD^+ to NADH photometrically at 340 nm. A blank measurement was also read for every compound in the absence of IMPDH as a pre-read. These pre-read values were finally employed as a filter along with the % inhibition of IMPDH II at 10 μM. A pre-read of less than or equal to 0.4 and an inhibition of greater than 50 % were used for filtration of HTS hits from the primary screen. All these hits were clustered using maximum common substructure (MCS) formalism as implemented in the MedChemStudio. This resulted in 425 classes and 1,044 singletons. The classes were further filtered by employing the cut-off for inhibition to greater than 60 %, drug-likeness and frequent hitters. The criteria for filtration of singletons were set more stringent by using inhibition cut-off of greater than 80 %, molecular weight between 300 and 500 D, drug-likeness and frequent hitters. The filtered hits, thus obtained, from classes and singletons were merged along with 3 reference compounds from Vertex and were subsequently used for re-testing and determination of IC_{50} values. The dose–response inhibition of IMPDH II by the reference compounds **2A**, **2B** and **2D** is shown in Fig. 11. Similarly, Fig. 12a–c depict the dose-dependent inhibition of IMPDH II by representative HTS hits (Fig. 10) along with one reference compound **1**. The scheme for clustering and filtration is given in Fig. 5. Figure 6 shows the frequency distribution of % IMPDH II inhibition of the hits resulting from primary screen, clustering and filtration as described above. Similarly, in Fig. 7, frequency distribution of % IMPDH II inhibition—classes versus singletons is shown. We then plotted the common physicochemical property distribution of the HTS hits such as molecular weight (Fig. 8a), AlogP (Fig. 8b), number of H-bond acceptors (Fig. 9a), number of H-bond donors (Fig. 9b) and lastly number of rotatable bonds (Fig. 9c).

In the re-testing or hit confirmation phase, 900 compounds which showed IC_{50} less than 5 μM were used for classification based on MCS approach. This exercise resulted in 90 classes and 7 singletons. A careful observation revealed 7 interesting classes which showed emerging SAR trends. The average ligand efficiency (LE) for each class was computed as a ratio of pIC_{50}/Number of heavy atoms and was used for further prioritization of these 7 classes.

HTS hits

The structures of the representative members of the interesting classes with corresponding IMPDH II inhibitory potencies are shown in Fig. 10. Class C1 (18 members)

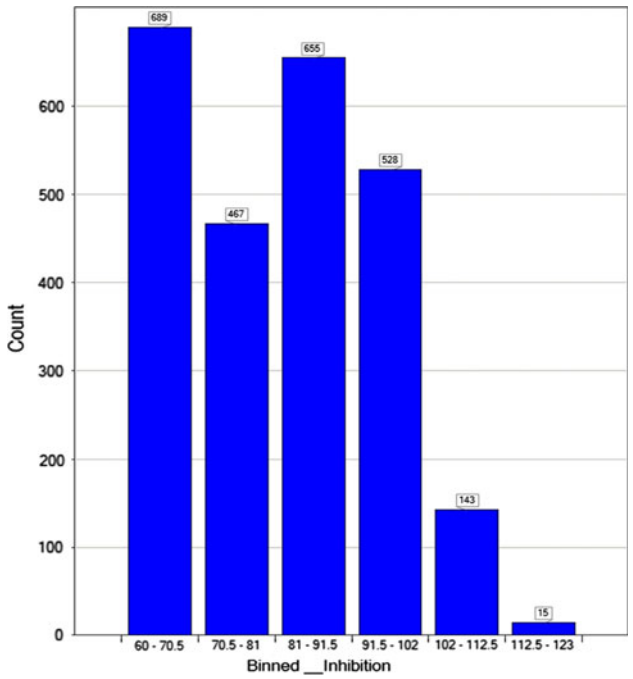

Fig. 6 Frequency distribution of % IMPDH II inhibition. The height of a bar represents No. of records. The x-axis is binned into 6 bins. The *labels* show the height of each *bar*

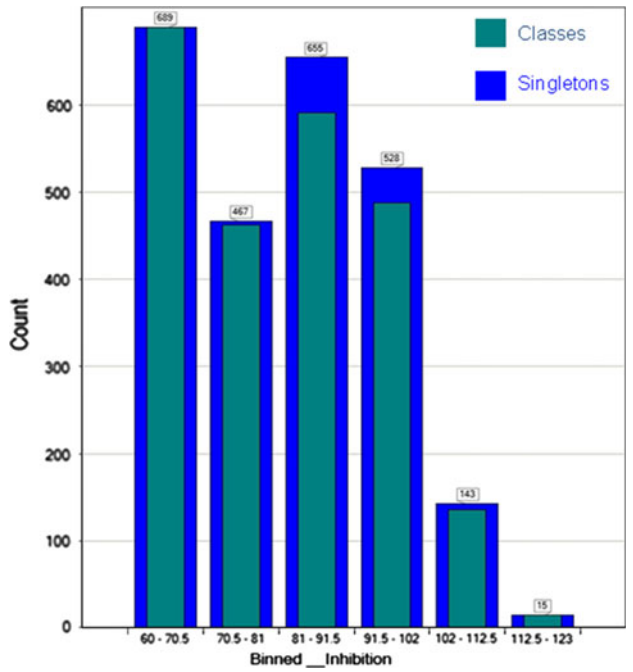

Fig. 7 Frequency distribution of % IMPDH II inhibition: classes versus singletons. The height of a *bar* represents No. of records. The x-axis is binned into 6 bins. The *labels* show the height of each *bar*

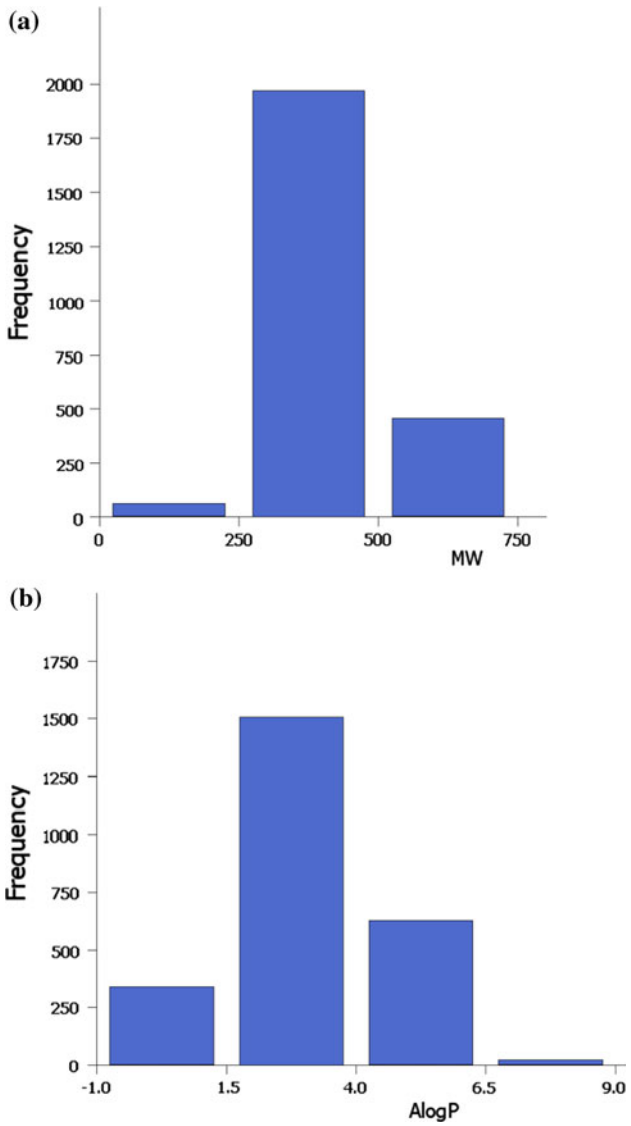

Fig. 8 Frequency distribution of **a** molecular weight (MW) and **b** AlogP among IMPDH II hits. The height of a *bar* represents number of records

was the largest of these classes with average LE of 0.272. The IC_{50} values range from 0.25 to 26.38 μM. All the compounds in this class (except two) possessed 2-(2-pyridylmethylsulfinyl)-1H-benzimidazole as the substructure which is also found in proton pump inhibitors (PPIs) such as omeprazole. By virtue of the tricoordinated sulfinyl sulfur in a pyramidal shape, compounds with this substructure are likely to exist as racemates. No further attempt was made to investigate the IMPDH II inhibitory activities of the R- and S-enantiomers. In terms of mini-SAR, the substituents on the benzimidazole ring significantly influenced the inhibitory potency compared to the substituents on the pyridine ring. The most potent compound of this class **4** (Fig. 10) has a H-bond acceptor duo (two –OMe groups) on neighboring aromatic ring carbons satisfying 2 acceptor feature requirements as outlined by

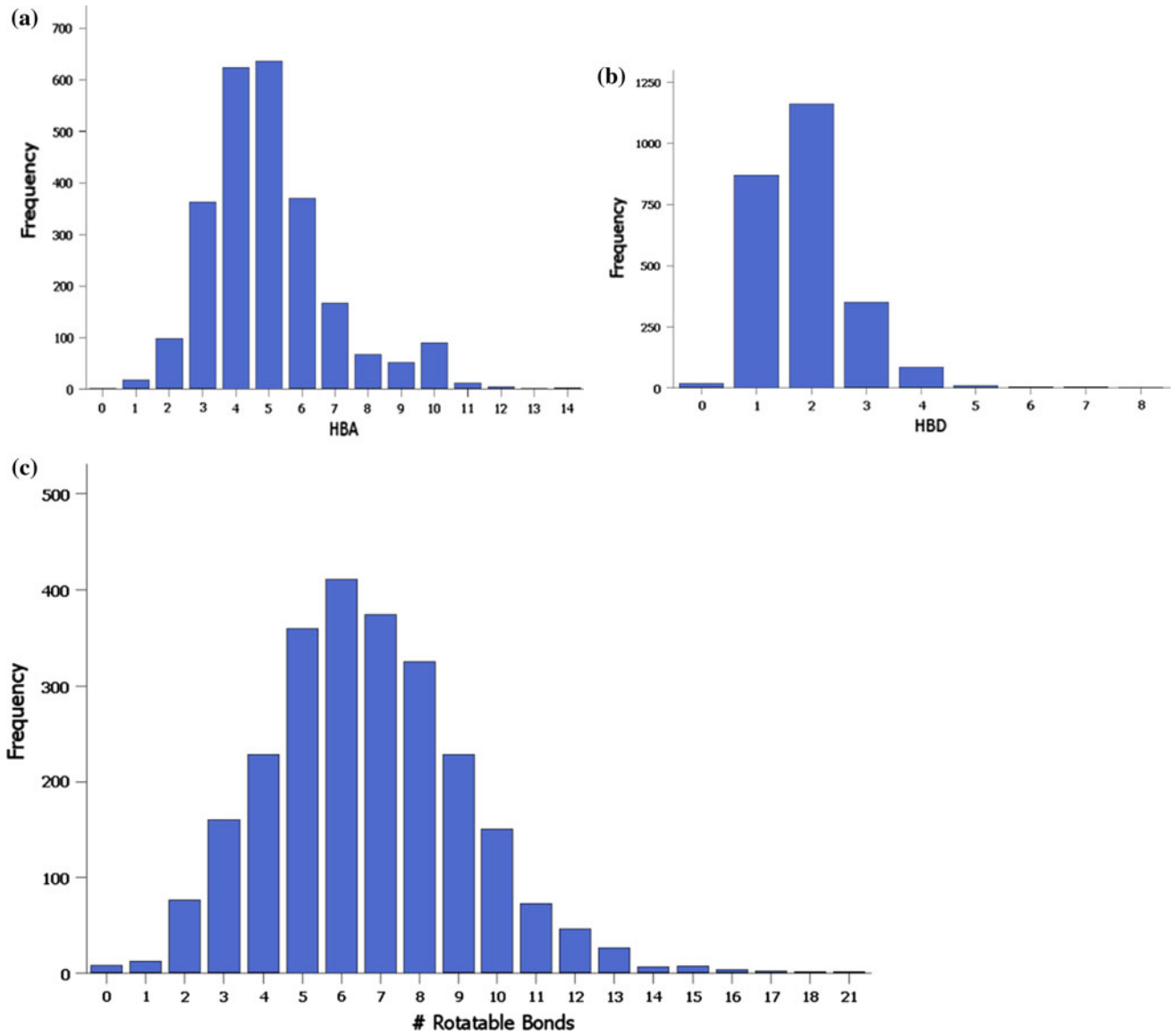

Fig. 9 Frequency distribution of **a** H-bond acceptors (HBA), **b** H-bond donors (HBD) and **c** number of rotatable bonds among IMPDH II hits. The height of a *bar* represents number of records

the pharmacophore (Fig. 4). Any change such as replacement of one –OMe by –Me or other bigger –OR (R = alkyl) group or an aromatic ring led to fall in potency (data not shown). Also, substitution on the pyridine ring by any group bigger than –OMe reduced the activity. It would be interesting to speculate the underlying mechanism of IMPDH II inhibition may be similar to the one exhibited by the PPIs wherein the chemical transformation in the drug under highly acidic conditions leads to disulfide bond formation with a Cys residue of the H^+/K^+-ATPase (Fig. 11).

Class C17 (benzamides) contained 3 members with average LE of 0.299. The most potent compound from this class (**6**, Fig. 10) possessed all 5 pharmacophoric features (AAADR). Reduction of the linker length (from 3 to 2 methylene) between the tertiary amine and the amide N reduced the potency by threefold (data not shown). Compound **7** (Fig. 10) is a bis-benzamide with a pendant Ph ring containing two acceptor features. No further information about the SAR of this class was available (Fig. 12).

Imidazo[1,2-a]pyridine formed the core structure of class C6 (7 members). The average LE for this class was 0.288. The eutomer of **9** (Fig. 10) was 2.5-fold more potent (data not shown). Conversion of ethanamide (**9**) to methyl carbamate (**8**) with simultaneous change in –Me group position on the Ph ring led to gain in potency. Substitution

Class: C1 (Members = 18)

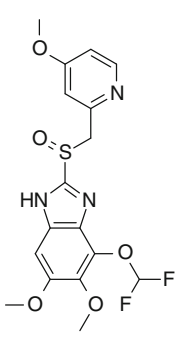

4
(IC_{50} = 0.25 μM)

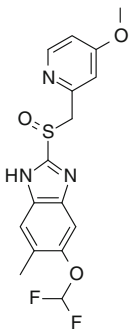

5
(IC_{50} = 1.23 μM)

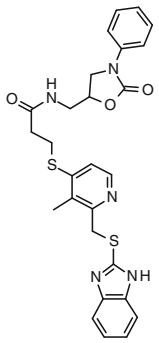

5a
(IC_{50} = 5.6 μM)

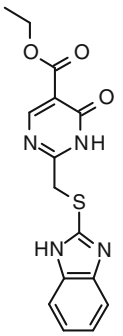

5b
(IC_{50} = 3.4 μM)

Class: C17 (Members = 3)

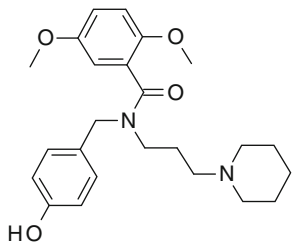

6
(IC_{50} = 0.16 μM)

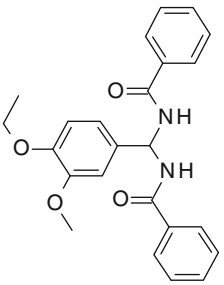

7
(IC_{50} = 1.81 μM)

Class: C6 (Members = 7)

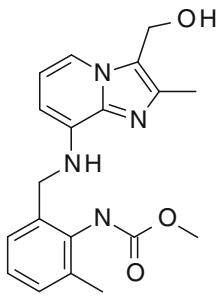

8
(IC_{50} = 0.4 μM)

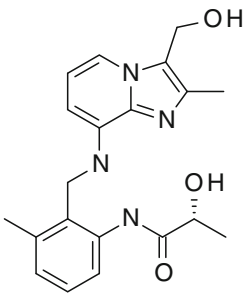

9
(IC_{50} = 0.73 μM)

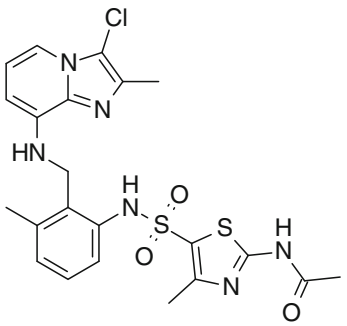

9a
(IC_{50} = 4.3 μM)

Fig. 10 HTS Hits—MCS[a] class representatives with corresponding IMPDH II inhibitory potencies

of the –OH group by $–NH_2$ group led to significant drop in potency (data not shown). No clear-cut SAR was observed in this class. This may be due to less number of compounds exhibiting inhibition under the current assay conditions.

Class C5 with 10 members exhibited average LE of 0.205. The prominent feature of Class C5 was the presence of at least 4 aromatic/heteroaromatic rings in the skeleton. Of the 10 members, seven contained 6-phenylnicotinamide substructure, while remaining three compounds were built around 2,4-diaminopyrimidine core. The IC_{50} values range from 0.54 to 19.81 μM. The most potent compound of the class belonged to the 2,4-diaminopyrimidine class (**15**, Fig. 10).

Class: C30 (Members = 2)

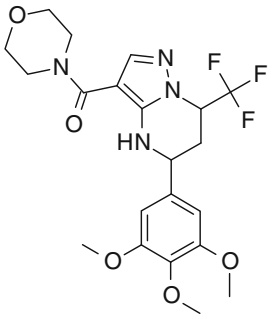

10
(IC_{50} = 1.89 μM)

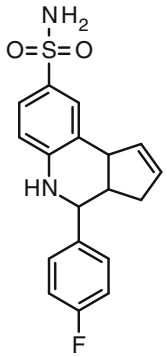

11
(IC_{50} = 3.38 μM)

Class: C18 (Members = 3)

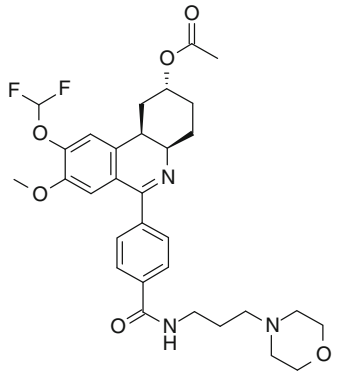

12
(IC_{50} = 0.45 μM)

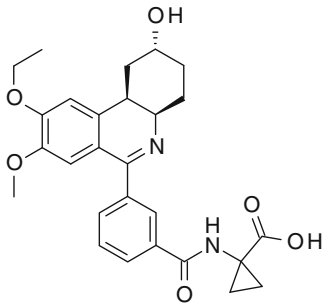

13
(IC_{50} = 3.12 μM)

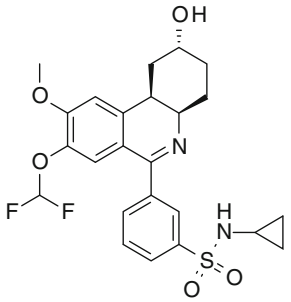

14
(IC_{50} = 7.95 μM)

Class: C5 (Members = 10)

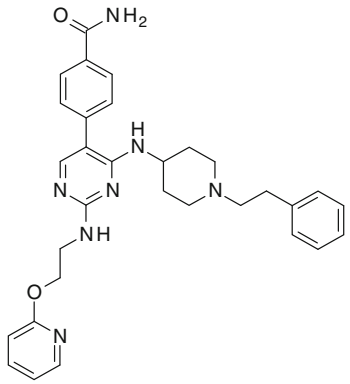

15
(IC_{50} = 0.54 μM)

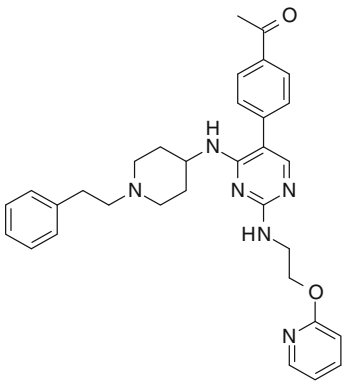

16
(IC_{50} = 4.8 μM)

Fig. 10 continued

Fig. 10 continued

Class: C11 (Members = 4)

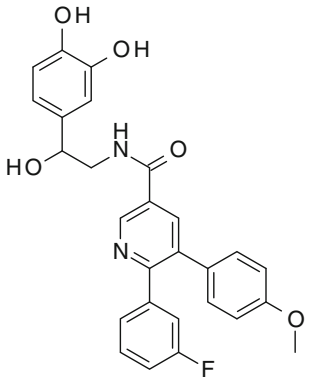

17
(IC_{50} = 8.2 μM)

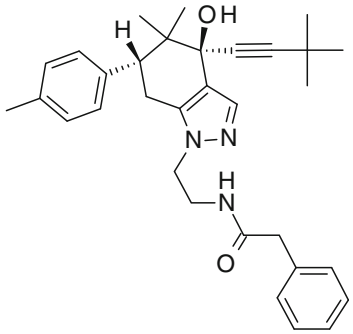

18
(IC_{50} = 4.7 μM)

[a] MCS: Maximum common substructure

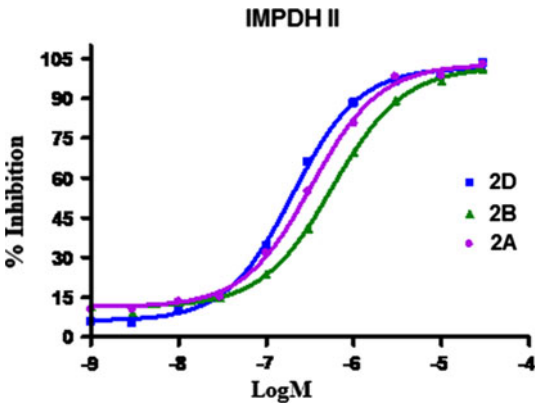

Fig. 11 The dose-dependent inhibition of IMPDH II by reference compounds VX-497 (**2A**), VX-148 (**2B**) and VX-944 (**2D**). Results are shown as mean values of triplicate samples in a single experiment

Another interesting class C18 (3 members, average LE = 0.207) had hexhydrophenanthridine core. Compound **12**, the most potent in the class, bore a masked hydroxyl group. Two neighboring H-bond acceptors (**12–14**, Fig. 10) on the core along with pendant 4-substituted benzamide containing a side chain were the common features in these molecules. Unmasking the hydroxyl group resulted into ~sixfold drop in potency. Further support for a meaningful SAR was not available for this class of compounds.

Classes C30 (2 members, average LE = 0.272) and C11 (4 members, average LE = 0.184) were comprised of compounds which lacked clear SAR due to structural diversity within the class and the smaller number of the constituent members of each class.

In general, all the 7 classes described above represent novel chemotypes resulted from an extensive virtual and experimental HTS campaign. Majority of these compounds would fall in two broad structural categories—(hetero)aromatic amides and sulfi(a)nyl benzimidazoles. Only representative compounds from each class were shown in Fig. 10. The analytical data of these compounds has been documented in the Experimental section. The ^{1}H-NMR spectra and/or HRMS or LC–MS data of few select compounds 4, 5, 5a, 5b, 8, 9, 9a, 10, 11–18 are given in the Electronic Suppementary Material.

Conclusions

Our attempts of discovering new IMPDH inhibitors culminated in 7 novel, structurally diverse chemical classes in a systematic ligand-based virtual screening followed by experimental HTS of 50,000 compounds. Of these, ~900 compounds showed IMPDH II IC_{50} less than 5 μM. Further inclusion of some compounds in the hit confirmation phase helped us deducing mini-SAR for some of these interesting classes. The compounds in the largest class had structural features strikingly similar to PPIs (e.g., omeprazole). Most of the compounds in other classes could be generically classified as (hetero)aromatic amides. The pharmacophore-based virtual screening coupled to similarity-based criteria, in our opinion, performed well in terms of identifying new chemotypes (hit rate 0.018). These newly identified IMPDH II inhibitors may serve as starting points for a drug discovery program. Further investigations such as selectivity, early

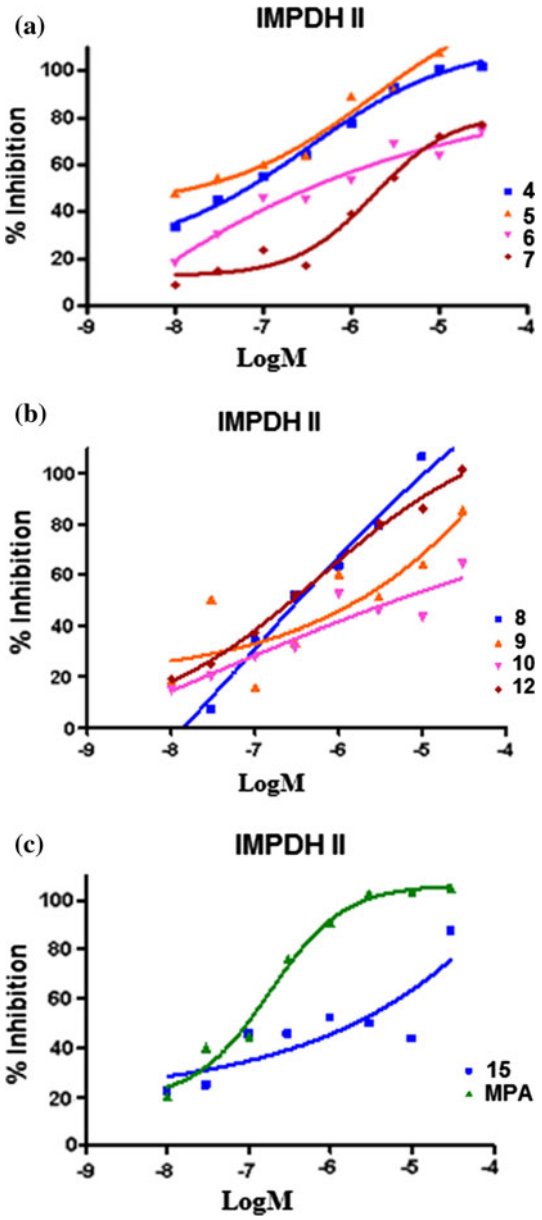

Fig. 12 The dose-dependent inhibition of IMPDH II by few IMPDH inhibitors including MPA. Results are shown as mean values of triplicate samples in a single experiment

ADME, toxicity, etc., of these inhibitors would certainly help prioritizing one class over the other going ahead.

Analytical data of the HTS hits

4-(Difluoromethoxy)-5,6-dimethoxy-2-[(4-methoxy-2-pyridyl)methylsulfinyl]-1H-benzimidazole (4)

Purity (HPLC): >98 %; ^{1}H-NMR (300 MHz, DMSO-d6)δ ppm 13.72 (brs, 1H), 8.33 (d, $J = 5.7$ Hz, 1H), 7.53 (brs, 1H), 7.00 (brs, 1H), 6.83–6.97 (m, 2H), 4.68–4.74 (m, 2H), 3.88 (s, 3H), 3.66–3.86 (m, 6H); LC–MS (ESI) [MH$^+$]: 414.08; HRMS (ESI) [MH$^+$] calcd for $C_{17}H_{18}F_2N_3O_5S$ 414.0925, found 414.0930.

5-(Difluoromethoxy)-2-[(4-methoxy-2-pyridyl) methylsulfinyl]-6-methyl-1H-benzimidazole (5)

Purity (HPLC): >99 %; ^{1}H-NMR (300 MHz, DMSO-d6)δ ppm 8.32 (d, $J = 5.7$ Hz, 1H), 7.55 (brs, 1H), 7.42 (brs, 1H), 6.98 (s, 1H), 6.64–6.96 (m, 2H), 4.59–4.73 (m, 2H), 3.74 (s, 3H), 2.35 (s, 3H); LC–MS (ESI) [MH$^+$]: 368.08; HRMS (ESI) [MH$^+$] calcd for $C_{16}H_{16}F_2N_3O_3S$ 368.0875, found 368.0875.

3-[[2-(1H-Benzimidazol-2-ylsulfanylmethyl)-3-methyl-4-pyridyl]sulfanyl]-N-[(2-oxo-3-phenyl-oxazolidin-5-yl)methyl]propanamide (5a)

Purity (HPLC): 91 %; ^{1}H-NMR (300 MHz, DMSO-d6)δ ppm 8.55 (t, 1H), 8.47 (d, $J = 6.0$ Hz, 1H), 7.67 (dd, $J = 6.2$, 3.2 Hz, 2H), 7.50-7.62 (m, 3H), 7.30–7.50 (m, 4H), 7.16 (d, $J = 7.6$ Hz, 1H), 5.02 (s, 2H), 4.81 (m, 1H), 3.83 (dd, J = 9.3, 6.6 Hz, 2H), 3.47–3.67 (m, 2H), 3.40 (t, $J = 6.8$ Hz, 2H), 2.65 (t, $J = 6.8$ Hz, 2H), 2.33 (s, 3H); LC–MS (ESI) [MH$^+$]: 534.33; HRMS (ESI) [MH$^+$] calcd for $C_{27}H_{28}N_5O_3S_2$ 534.1624, found 534.1628.

Ethyl 2-(1H-benzimidazol-2-ylsulfanylmethyl)-6-oxo-1H-pyrimidine-5-carboxylate (5b)

Purity (HPLC): >99 %; ^{1}H-NMR (300 MHz, DMSO-d6)δ ppm 8.34 (s, 1H), 7.52 (dd, $J = 6.2$, 3.2 Hz, 2H), 7.25 (dd, $J = 6.0$, 3.3 Hz, 2H), 4.35–4.72 (s, 2H), 4.14 (q, $J = 7.2$ Hz, 2H), 1.17 (t, $J = 7.0$ Hz, 3H); LC–MS (ESI) [MH$^+$]: 331.17; HRMS (ESI) [MH$^+$] calcd for $C_{15}H_{15}N_4O_3S$ 331.0859, found 331.0861.

MethylN-[2-[[[3-(hydroxymethyl)-2-methyl-imidazo [1,2-a]pyridin-8-yl]amino]methyl]-6-meth-yl-phenyl]carbamate (8)

Purity (HPLC): >90 %; ^{1}H-NMR (300 MHz, DMSO-d6)δ ppm 8.94 (s, 1H), 7.62 (d, $J = 6.8$ Hz, 1H), 6.94–7.27 (m, 3H), 6.62 (t, $J = 7.0$ Hz, 2H), 5.85 (d, $J = 7.6$ Hz, 1H), 5.06 (t, $J = 5.3$ Hz, 1H), 4.75 (d, $J = 4.9$ Hz, 2H), 4.43 (d, $J = 5.7$ Hz, 2H), 3.73 (s, 3H), 2.40 (s, 3H), 2.25 (s, 3H); LC–MS (ESI) [MH$^+$]: 355.33; HRMS (ESI) [MH$^+$] calcd for $C_{19}H_{23}N_4O_3$ 355.1765, found 355.1765.

(2R)-2-Hydroxy-N-[2-[[[3-(hydroxymethyl)-2-methyl-imidazo[1,2-a]pyridin-8-yl]amino]methyl]-3-methyl-phenyl]propanamide (9)

Purity (HPLC): 97 %; ^{1}H-NMR (300 MHz, DMSO-d6)δ ppm 9.65 (s, 1H), 7.65 (d, $J = 6.8$ Hz, 1H), 7.37 (d,

$J = 7.2$ Hz, 1H), 7.22 (t, $J = 7.7$ Hz, 1H), 7.08 (d, $J = 7.2$ Hz, 1H), 6.72 (t, $J = 7.2$ Hz, 1H), 6.32 (d, $J = 7.2$ Hz, 1H), 5.81 (d, $J = 4.5$ Hz, 1H), 5.55 (t, $J = 5.5$ Hz, 1H), 5.02 (t, $J = 5.3$ Hz, 1H), 4.69 (d, $J = 4.9$ Hz, 2H), 4.30 (d, $J = 5.3$ Hz, 2H), 4.11 (dd, $J = 6.8$, 3.8 Hz, 1H), 2.34 (s, 3H), 2.28 (s, 3H), 1.26 (d, $J = 6.8$ Hz, 3H); LC–MS (ESI) [MH^+]: 369.33; HRMS (ESI) [MH^+] calcd for $C_{20}H_{25}N_4O_3$ 369.1921, found 369.1921.

N-[5-[[2-[[(3-chloro-2-methyl-imidazo[1,2-a]pyridin-8-yl)amino]methyl]-3-methyl-phenyl]sulfa-moyl]-4-methyl-thiazol-2-yl]acetamide (9a)

Purity (HPLC): >98 %; ^{1}H-NMR (300 MHz, DMSO-d6)δ ppm 12.41 (s, 1H), 9.94 (s, 1H), 7.47 (d, $J = 6.4$ Hz, 1H), 7.05–7.25 (m, 2H), 6.77 (t, $J = 7.2$ Hz, 1H), 6.66 (dd, $J = 6.4$, 2.6 Hz, 1H), 6.24 (d, $J = 7.9$ Hz, 1H), 5.53 (t, 1H), 4.39 (d, $J = 5.3$ Hz, 2H), 2.28 (s, 3H), 2.23 (s, 3H), 2.09 (s, 3H), 2.03 (s, 3H); LC–MS (ESI) [MH^+]: 519.25; HRMS (ESI) [MH^+] calcd for $C_{21}H_{26}F_3N_4O_4$ 519.1028, found 519.1034.

Morpholino-[7-(trifluoromethyl)-5-(3,4,5-trimethoxyphenyl)-4,5,6,7-tetrahydropyrazolo-[1,5-a]pyrimidin-3-yl]methanone (10)

HRMS (ESI) [MH^+] calcd for $C_{21}H_{26}F_3N_4O_4$ 471.1852, found 471.1850.

4-(4-Fluorophenyl)-3a,4,5,9b-tetrahydro-3H-cyclopenta[c]quinoline-8-sulfonamide (11)

Purity (HPLC): 95 %; ^{1}H-NMR (300 MHz, DMSO-d6)δ ppm 7.46–7.75 (m, 2H), 7.40 (dd, $J = 8.3$, 2.3 Hz, 1H), 7.28 (t, $J = 8.9$ Hz, 2H), 7.02 (s, 1H), 6.86 (d, $J = 8.7$ Hz, 1H), 6.44 (s, 1H), 5.95 (d, $J = 1.5$ Hz, 1H), 5.69 (d, $J = 4.9$ Hz, 1H), 4.71 (d, $J = 3.0$ Hz, 1H), 4.13 (d, $J = 8.7$ Hz, 1H), 2.99 (d, $J = 9.1$ Hz, 1H), 2.07 (m, 1H), 1.60–1.75 (dd, 1H); LC–MS (ESI) [MH^+]: 345.25.

[(2R,4aR,10bR)-9-(Difluoromethoxy)-8-methoxy-6-[4-(3-morpholinopropylcarbamoyl)-phenyl]-1,2,3,4,4a,10b-hexahydrophenanthridin-2-yl] acetate (12)

Purity (HPLC): 97 %; ^{1}H-NMR (300 MHz, DMSO-d6)δ ppm 8.60 (t, $J = 5.7$ Hz, 1H), 7.94 (d, $J = 8.7$ Hz, 2H), 7.67 (d, $J = 8.3$ Hz, 2H), 7.28 (s, 1H), 7.21 (s, 1H), 6.87 (s, 1H), 4.87 (brs, 1H), 3.68 (s, 4H), 3.52–3.63 (m, 4H), 3.29–3.35 (m, 4H), 2.95–3.10 (m, 1H), 2.30–2.45 (m, 6H), 2.09 (s, 3H), 1.46–1.77 (m, 6H); LC–MS (ESI) [MH^+]: 586.50; HRMS (ESI) [MH^+] calcd for $C_{31}H_{38}F_2N_3O_6$ 586.2721, found 586.2723.

1-[[3-[(2R,4aR,10bR)-9-Ethoxy-2-hydroxy-8-methoxy-1,2,3,4,4a,10b-hexahydrophenan-thridin-6-yl]benzoyl]amino]cyclopropanecarboxylic acid (13)

Purity (HPLC): 90 %; LC–MS (ESI) [M-H]$^+$: 477.42; HRMS (ESI) [MH^+] calcd for $C_{27}H_{31}N_2O_6$ 479.2176, found 479.2177.

3-[(2R,4aR,10bR)-8-(Difluoromethoxy)-2-hydroxy-9-methoxy-1,2,3,4,4a,10b-hexahydro-phenanthridin-6-yl]-N-cyclopropyl-benzenesulfonamide (14)

Purity (HPLC): 90 %; ^{1}H-NMR (300 MHz, DMSO-d6)δ ppm 8.01 (d, $J = 2.6$ Hz, 1H), 7.86–7.97 (m, 2H), 7.65–7.80 (m, 2H), 7.15 (s, 1H), 6.89 (s, 1H), 4.58 (d, $J = 3.0$ Hz, 1H), 3.93 (s, 3H), 3.75–3.90 (m, 2H), 3.61 (d, $J = 4.2$ Hz, 1H), 2.07–2.30 (m, 2H), 1.80–1.95 (m, 1H), 1.57 (brs, 4H), 1.23 (brs, 2H), 0.99 (t, $J = 7.4$ Hz, 1H); LC–MS (ESI) [MH^+]: 493.33; HRMS (ESI) [MH^+] calcd for $C_{24}H_{27}F_2N_2O_5S$ 493.1603, found 493.1598.

4-[4-[(1-phenethyl-4-piperidyl)amino]-2-[2-(2-pyridyloxy)ethylamino]pyrimidin-5-yl]benzamide (15)

Purity (HPLC): 90 %; ^{1}H-NMR (300 MHz, DMSO-d6) δ ppm 8.15 (dd, $J = 5.1$, 1.3 Hz, 1H), 7.97 (brs, 1H), 7.81–7.95 (m, 3H), 7.64–7.76 (m, 2H), 7.61 (d, $J = 5.3$ Hz, 1H), 7.36-7.55 (m, 2H), 7.33 (brs, 1H), 7.11–7.31 (m, 3H), 6.88–7.04 (m, 1H), 6.64–6.88 (d, 2H), 5.88 (brs, 1H), 4.39 (t, $J = 6.0$ Hz, 2H), 3.91 (brs, 1H), 3.48–3.75 (m, 2H), 3.38–3.48 (m, 1H), 2.81 (d, J = 9.8 Hz, 2H), 2.62–2.76 (m, 2H), 2.36–2.47 (m, 2H), 1.96 (brs, 2H), 1.80 (d, $J = 9.8$ Hz, 2H), 1.47 (d, J = 9.1 Hz, 1H); LC–MS (ESI) [MH^+]: 538.33; HRMS (ESI) [MH^+] calcd for $C_{31}H_{36}N_7O_2$ 538.2917, found 538.2925.

1-[4-[4-[(1-Phenethyl-4-piperidyl)amino]-2-[2-(2-pyridyloxy)ethylamino]pyrimidin-5-yl]phenyl]-ethanone (16)

Purity (HPLC): 90 %; ^{1}H-NMR (300 MHz, DMSO-d6) δ ppm 8.07–8.28 (m, 1H), 7.98 (d, $J = 8.3$ Hz, 2H), 7.60–7.84 (m, 2H), 7.49 (d, $J = 8.3$ Hz, 2H), 7.09–7.33 (m, 4H), 6.91–7.04 (m, 1H), 6.89 (brs, 1H), 6.61–6.87 (m, 1H), 5.98 (brs, 1H), 4.39 (t, $J = 6.0$ Hz, 2H), 3.91 (brs, 1H), 3.62 (m, 2H), 2.83 (brs, 1H), 2.80 (brs, 1H), 2.61–2.73 (m, 2H), 2.58 (s, 3H), 2.40–2.52 (m, 2H),1.97 (d, $J = 7.2$ Hz, 2H), 1.80 (d, $J = 9.8$ Hz, 2H), 1.47 (d, $J = 9.4$ Hz, 2H); LC–MS (ESI) [MH^+]: 537.33; HRMS (ESI) [MH^+] calcd for $C_{32}H_{37}N_6O_2$ 537.2971, found 537.2973.

N-[2-(3,4-Dihydroxyphenyl)-2-hydroxy-ethyl]-6-(3-fluorophenyl)-5-(4-methoxyphenyl)pyridine-3-carboxamide (17)

Purity (HPLC): >99 %; ^{1}H-NMR (300 MHz, DMSO-d6) δ ppm 9.01 (d, $J = 2.3$ Hz, 1H), 8.75–8.85 (m, 1H), 8.20 (d, $J = 1.9$ Hz, 1H), 7.32 (d, $J = 7.9$ Hz, 1H), 7.04–7.24 (m, 5H), 6.93 (d, $J = 9.1$ Hz, 2H), 6.79 (d, $J = 1.9$ Hz, 1H), 6.67 (d, $J = 7.9$ Hz, 1H), 6.60 (dd, $J = 7.9$, 1.9 Hz, 1H), 5.31 (brs, 1H), 4.61 (brs, 1H), 3.75 (s, 3H), 2.08 (s, 1H); LC–MS (ESI) [MH^+]: 475.42; HRMS (ESI) [MH^+] calcd for $C_{27}H_{24}FN_2O_5$ 475.1664, found 475.1664.

N-[2-[(4S,6R)-4-(3,3-Dimethylbut-1-ynyl)-4-hydroxy-5,5-dimethyl-6-(p-tolyl)-6,7-dihydroinda-zol-1-yl]ethyl]-2-phenylacetamide (18)

Purity (HPLC): >94 %; ^{1}H-NMR (300 MHz, DMSO-d6) δ ppm 8.02–8.39 (t, 2H), 7.45 (s, 1H), 7.08–7.37 (m, 9H), 5.47 (s, 1H), 3.99 (t, $J = 6.4$ Hz, 2H), 3.35–3.45 (t, 2H), 3.26–3.35 (m, 1H), 2.80–2.95 (m, 1H), 2.65 (d, $J = 5.3$ Hz, 1H), 2.31 (s, 3H), 1.20 (s, 9H), 0.80 (s, 3H), 0.75 (s, 3H); LC–MS (ESI) [MH^+]: 480.42.

Acknowledgments The authors are thankful to Jürgen Volz and colleagues for providing the HRMS data, Katharina Rossbach and colleagues for providing HTS samples, Digambar Bankar, Pritee Kulkarni, Anuja Patil, Sunil Chavan and the Analytical Department, Global Discovery, Mumbai, for their help in recording the required analytical Data.

References

1. Ciustea M, Silverman JEY, Shudofsky AMD, Ricciardi RP (2008) Identi-fication of non-nucleoside DNA synthesis inhibitors of vaccinica virus by high-throughput screening. J Med Chem 51:6563–6570
2. Mattila E, Ivaska J (2011) High-throughput methods in identification of protein tyrosine phosphatase inhibitors and activators. Anticancer Agents Med Chem 11:141–150
3. Cheng J-F, Zapf J, Takedomi K, Fukushima C, Ogiku T, Zhang S-H, Yang G, Sakurai N, Barbosa M, Jack R, Xu K (2008) Combination of virtual screening and high throughput gene profiling for identification of novel liver X receptor modulators. J Med Chem 51:2057–2061
4. Polgár T, Baki A, Szendrei GI, Keserű GM (2005) Comparative virtual and experimental high-throughput screening for glycogen synthase kinase-3β inhibitors. J Med Chem 48:7946–7959
5. Crabtree GW, Henderson JF (1971) Rate-limiting steps in the interconversion of purine ribonucleotides in Ehrlich ascites tumor cells in vitro. Cancer Res 31:985–991
6. Jackson RC, Weber G, Morris HP (1975) IMP dehydro-genase, an enzyme linked with proliferation and malignancy. Nature 256:331–333
7. Franchetti P, Grifantini M (1999) Nucleoside and non-nucleoside IMP dehydrogenase inhibitors as antitumor and antiviral agents. Curr Med Chem 6:599–614
8. Ratcliffe AJ (2006) Inosine 5′-monophosphate dehydrogenase inhibitors for the treatment of autoimmune diseases. Curr Opin Drug Discov Dev 9:595–605
9. Braun-Sand SB, Peetz M (2010) Inosine monophosphate dehydrogenase as a target for antiviral, anticancer, antimicrobial and immunosuppressive therapeutics. Future Med Chem 2:81–92
10. Sollinger HW (1995) Mycophenolate mofetil for the prevention of acute rejection in primary cadaveric renal allograft recipients (US Renal Transplant Mycophenolate Mofetil Study Group). Transplantation 60:225–232
11. Suite Schrödinger (2011) is available from Schrödinger. LLC, New York 2011
12. Sintchak MD, Fleming MA, Futer O, Raybuck SA, Chambers SP, Caron PR, Murcko MA, Wilson KP (1996) Structure and mechanism of inosine mono-phosphate dehydrogenase in complex with the immunosuppressant mycophenolic acid. Cell 85:921–930
13. Sintchak MD, Nimmesgern E (2000) The structure of insoine 5′-monophosphate dehydrogenase and the design of novel inhibitors. Immunopharmacol 47:163–184
14. Phase, version 3.3, Schrödinger, LLC, New York, NY, 2011
15. Dixon SL, Smondyrev AM, Knoll EH, Rao SN, Shaw DE, Friesner RA (2006) PHASE: a new engine for pharmacophore perception, 3D QSAR model development, and 3D database screening. 1. Methodology and preliminary results. J Comput Aided Mol Des 20:647–671
16. Canvas, version 1.4 (Schrodinger Suite 2011) Schrödinger, LLC, New York
17. Duan J, Dixon SL, Lowrie JF, Sherman W (2010) Analysis and comparison of 2D fingerprints: insights into database screening performance using eight finger-print methods. J Mol Graph Model 29:157–170
18. FTress, version 2.4 (2012) BioSolveIT GmbH, An der Ziegelei 75, 53757 St. Augustin, Germany
19. Rarey M, Dixon JS (1998) Feature trees: a new molecular similarity measure based on tree matching. J Comput Aided Mol Des 12:471–490
20. SpotFire® DecisionSite®9.1.1 version 19.12.1011 TIBCO Spotfire, Somerville, MA
21. Sastry M, Lowrie JF, Dixon SL, Sherman W (2010) Large-scale systematic analysis of 2D fingerprint methods and parameters to improve virtual screening enrichments. J Chem Inf Model 50:771–784
22. Glide, version 5.7 (Schrodinger Suite 2011) Schrödinger, LLC, New York
23. Friesner RA, Banks JL, Murphy RB, Halgren TA, Klicic JJ, Mainz DT, Repasky MP, Knoll EH, Shaw DE, Shelley M, Perry JK, Francis P, Shenkin PS (2004) Glide: a new approach for rapid, accurate docking and scoring. 1. Method and assessment of docking accuracy. J Med Chem 47:1739–1749
24. Halgren TA, Murphy RB, Friesner RA, Beard HS, Frye LL, Pollard WT, Banks JL (2004) Glide: a new approach for rapid, accurate docking and scoring. 2. Enrichment factors in database screening. J Med Chem 47:1750–1759
25. Friesner RA, Murphy RB, Repasky MP, Frye LL, Greenwood JR, Halgren TA, Sanschagrin PC, Mainz DT (2006) Extra precision glide: docking and scoring incorporating a model of hydrophobic enclosure for protein-ligand complexes. J Med Chem 49: 6177–6196
26. Yang N, Wang J, Li J, Wang Q-H, Wang Y, Cheng M-S (2011) A three-dimensional pharmacophore model for IMPDH inhibitors. Chem Biol Drug Des 78:175–182